

Chapter 13

Solar Activity in the Past and Its Impacts on Climate



Hiroko Miyahara, Ayumi Asai, and Satoru Ueno

13.1 Long-Term Variations in Solar Irradiance and Ultraviolet Radiation and Their Estimation

The Sun is far away from the Earth, at a distance of approximately 150 million km. However, the Earth receives an enormous amount of sunlight and electromagnetic radiation from the Sun, under which life on Earth is nurtured. The total light energy received by the Earth is 1361 W/m^2 when all wavelengths of the radiation are integrated. This is called total solar irradiance (TSI). The top panel of Fig. 13.1 shows the variations in the TSI over the past 40 years (Hansen et al. 2013). There are several sharp decrements in the TSI variations; these are not due to observation errors, but rather to the appearance of a large sunspot or multiple sunspots. As shown in Fig. 12.1 and the bottom panel of Fig. 13.1, the sunspot number increases and decreases periodically in a cycle of approximately 11 years. Overall, the variations in the sunspot number and TSI are synchronized. Specifically, the Sun is brighter in the solar maximum than it is in the solar minimum. However, the range of fluctuation is only 0.1% (1/1000), which is at most approximately $\pm 1 \text{ W/m}^2$ in one solar cycle (i.e., 11 years). The reason the TSI is called the “solar constant” is that the variations are very small.

In addition to visible light, which humans can see, the Sun emits light in a wide range of wavelengths, including short wavelengths, such as ultraviolet (UV) rays, X-rays, and γ -rays, and long wavelengths, such as infrared rays and radio waves. The intensity of the radiation at each wavelength is called the spectral solar irradiance (SSI) (Fig. 13.2a). Because the atmosphere of the Earth absorbs various wavelengths

H. Miyahara (✉)

Humanities and Sciences/Museum Careers, Musashino Art University, Tokyo, Japan
e-mail: miyahara@musabi.ac.jp

A. Asai · S. Ueno

Astronomical Observatory, Graduate School of Science, Kyoto University, Kyoto, Japan

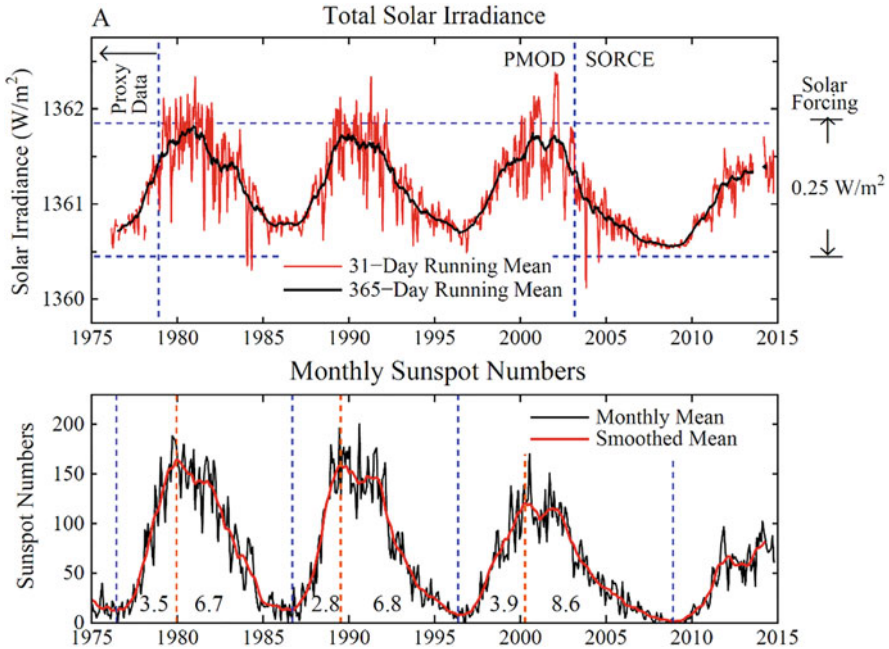


Fig. 13.1 TSI (top panel) versus sunspot number (bottom panel). (Hansen et al. 2013: https://commons.wikimedia.org/wiki/File:Changes_in_total_solar_irradiance_and_monthly_sunspot_numbers_1975-2013.png)

and the amount of absorption significantly varies depending on the atmospheric conditions, the TSI and the SSI must, in principle, be measured outside the atmosphere of the Earth using satellites. Although they have been measured using several instruments for a long time, the observed values of the TSI have been slightly different owing to the improvement in instrumentation. Therefore, to observe the long-term variability in the TSI, it is necessary to relate the TSI data from multiple satellites. However, even the variability in the TSI over the past 40 years is uncertain, ranging from almost no change to a gradual increase and a gradual decrease, depending on the calibration method for relating the data from different instruments (Solanki et al. 2013). During the period of extremely low solar activity (Maunder Minimum) between 1645 and 1715, the TSI has been also estimated to have declined, with estimates of the decrease ranging from 0.9 W/m^2 to 3 W/m^2 , depending on the model (Schrijver et al. 2011; Krivova et al. 2010; Steinhilber et al. 2009; Solanki et al. 2013). If the TSI was extremely low to the extent of the upper limit of the above range, it could explain the cold climate (mini-ice age) around the time of the Maunder Minimum.

In contrast to the TSI, the interest in the variability of the SSI, particularly of the solar UV radiation, has been increasing recently. Most of the light with wavelengths shorter than visible light is absorbed by the atmosphere of the Earth. As shown in Fig. 13.2b (Ermolli et al. 2013), the altitude of the atmosphere of the Earth at which

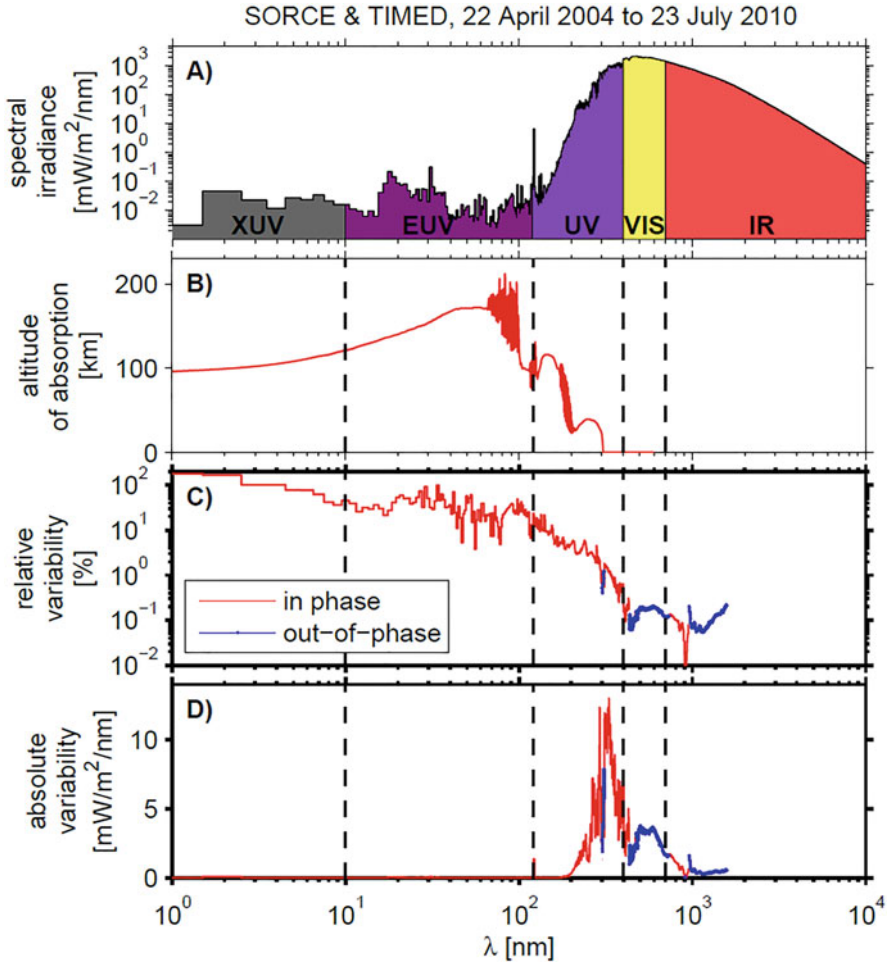


Fig. 13.2 (a) SSI, (b) characteristic altitude of absorption in the atmosphere of Earth for each wavelength, (c) relative variability in solar cycle variations inferred from measurements obtained between April 22, 2004, and July 23, 2010, (d) absolute variability. (Reprinted by Ermolli et al. (2013))

light is absorbed depends on its wavelength and corresponds to the thermosphere, mesosphere, and stratosphere. The solar UV radiation also varies synchronously with the solar activity cycle; however, its variability is much larger than that of the TSI (0.1%), ranging from 10% to 100% depending on the wavelength (Fig. 13.2c). The absolute amount of variability (Fig. 13.2d) also shows that the UV region accounts for a large proportion, suggesting that it is responsible for the variability in the TSI (e.g., Lean 1997). However, the long-term variability in the SSI also remains uncertain, because continuous satellite-based observations have been limited to recent years.

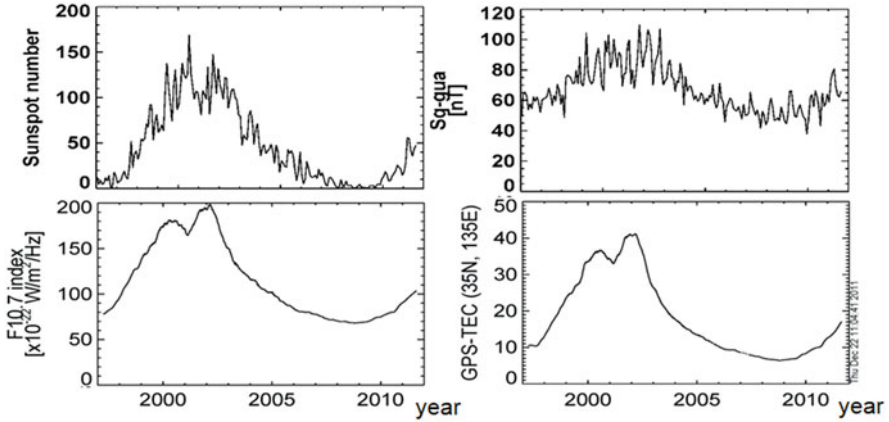


Fig. 13.3 Variations in sunspot number (upper left), solar radio F10.7 intensity (10.7 cm wavelength radio wave: lower left), geomagnetic Sq field (Guam station: upper right), and ionospheric total electron number over Japan by GPS satellite (lower right). (Courtesy of Dr. A. Shinbori)

Each layer of the atmosphere of the Earth that absorbs UV radiation responds sensitively to solar UV variations. Figure 13.3 shows the geomagnetic solar quiet daily variations (geomagnetic Sq field) (upper right) and the total electron content (TEC) (lower right) of the ionosphere. The geomagnetic Sq field is the amount of geomagnetic variations due to the electric current generated by the absorption of UV radiation of approximately 100–200 nm by the atmosphere of the Earth at an altitude of approximately 90–120 km. The TEC shows the variations in the number of electrons resulting from the ionization of the atmosphere of the Earth by UV radiation with a wavelength shorter than 50 nm in the upper ionosphere at high altitudes (approximately 200–500 km). The panels show the variations after subtracting specific variations of the Earth, such as seasonal changes, and it can be confirmed that both variations are synchronized with the variations in the sunspot number.

In the period when there is no (poor) direct observation data of solar UV by satellites, it is necessary to estimate its variations from other observation data. The solar UV radiation is emitted from the solar atmosphere—which is called the “chromosphere” and has a temperature of approximately 10,000 K—above the solar surface called the “photosphere.” Therefore, the variations in the sunspot number can be indicators of magnetic activity to some extent; however, it is insufficiently precise to estimate the activity of the solar chromosphere. In contrast, solar radio intensity F10.7 (the total amount of radio waves with a wavelength of 10.7 cm emitted from the entire surface of the Sun; lower left of Fig. 13.3) has been frequently used (Tapping and Charrois 1994). The F10.7 intensity is known to be sensitive to the chromosphere and correlates well with the sunspot number and other physical parameters of the solar activity (particularly those attributed to the chromosphere). In addition, it has been used as an indicator of the long-term UV radiation variability because of the stable observation records accumulated since

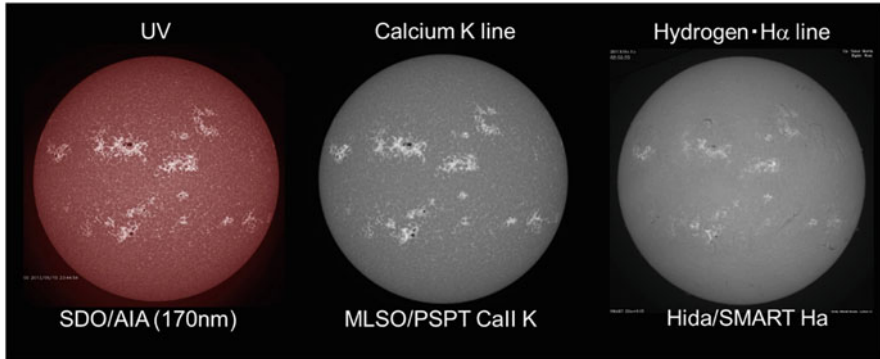


Fig. 13.4 Comparison of solar UV images (left: 171-nm image taken by SDO/AIA, National Aeronautics and Space Administration), calcium K-line image (middle: taken by Precision Solar Photometric Telescope at Hawaii Mauna Loa Solar Observatory), and H α -line image (right: taken by SMART at Hida Observatory, Kyoto University) on May 15, 2013

1947. In Japan, the Nobeyama Solar Radio Observatory of the National Astronomical Observatory of Japan (NAOJ) has been continuously observing the Sun in the microwave band (frequency 1–10 GHz, wavelength 3–30 cm) since 1957 (Shimojo et al. 2017), and microwaves show similar variations to the F10.7 intensity.

The solar minimum around 2008 (the transition period from the 23rd to the 24th solar cycle) was an “anomalous” minimum period with a remarkably low activity level in recent years, and the behaviors of the geophysical parameters used as indicators of the solar activity were different (Fröhlich 2009). In particular, the TSI and the UV-SSI showed a significant decrease, whereas radio emissions such as F10.7 did not decrease as much (and were comparable to those in earlier minima). Therefore, the solar UV radiation using the F10.7 intensity overestimates the UV radiation intensity, at least in this solar minimum period.

As mentioned earlier, solar UV radiation is mainly emitted from the solar atmosphere, called the chromosphere, at a temperature of approximately 10,000 K (Lean 1987). The left part of Fig. 13.4 is an image of the solar UV radiation (170 nm) taken by a UV imager, the Atmospheric Imaging Assembly (AIA) onboard the Solar Dynamics Observatory (SDO) satellite of NASA. The middle and right parts are solar images at spectral lines formed by the solar chromosphere in the visible light region. They are the calcium K-line image taken by the Mauna Loa Solar Observatory in Hawaii and the H α -line image by the Solar Magnetic Activity Research Telescope (SMART) at the Hida Observatory of Kyoto University, respectively. These images show very similar features, particularly their bright regions around sunspots (plages). A plage is a region of relatively high magnetic field strength (not as high as that of sunspots, but sufficiently higher than quiet regions) where magnetic field activity occurs.

Therefore, estimates of solar UV intensity based on solar chromosphere images are underway (e.g., Chatzistergos et al. 2019; Kakuwa and Ueno 2022). In the case of calcium and H α images, observation data spanning approximately 100 years have

been accumulated. As examples, observations of the calcium K line using glass plates have been made at Kyoto University since 1928 (Kitai et al. 2014), at the NAOJ since 1917 (Hanaoka 2013), and at Kodaikanal, India, since 1907 (Hasan et al. 2010). Other instances are those at the Mt. Wilson Observatory, U.S., since 1915 (Bertello et al. 2010), and at the Arcetri Observatory, Italy, since 1931 (Ermolli et al. 2009). Although these also do not directly represent solar UV intensity, the similarities between the UV and chromospheric images presented in Fig. 13.4 have led to estimates of the solar UV radiation (Bertello et al. 2010, Chatterjee Chatterjee et al. 2016), particularly focusing on the plage region. Furthermore, the calcium K line observations at the above observatories have different bandpass widths around the center of the absorption line. In particular, observations with narrower bandpass widths (e.g., Mt. Wilson Observatory) show a higher atmospheric layer than those with wider bandpass widths (e.g., Kodaikanal, Kyoto University), and it has been reported that they may be highly correlated with shorter wavelengths of light in the UV region (Foukal et al. 2009). However, the conversion (calibration) of densities of glass plate data to calcium K line intensities is still under development (Kakuwa and Ueno 2021), and the estimation of the solar UV radiation is difficult.

Regarding the geomagnetic Sq field, because it responds to a limited wavelength range, we could estimate the solar UV radiation from its variations. However, Elias et al. (2010) investigated the long-term variations in the geomagnetic Sq field of the Earth, and found that it shows a monotonic increasing trend even after subtracting the “variation due to solar activity.” Furthermore, they proposed that this increasing trend is related to the lower atmosphere, e.g., due to global warming. Comparatively, Shinbori et al. (2014) investigated the geomagnetic Sq field in more detail and over a longer period and reported a slightly decreasing trend. However, in the derivation, they used the sunspot number for the former (Elias et al. 2010) and the solar radio intensity F10.7 for the latter (Shinbori et al. 2014) to estimate the solar UV variability. Thus, we have not yet been able to accurately distinguish between the influence of solar UV radiation and the component of the variations specific to the atmosphere of the Earth, from the Sq variations. In this respect, more accurate SSI estimation in the UV region is also desired.

13.2 Detailed Analyses of Past Solar and Cosmic-Ray Variations

Concentrations of cosmic-ray-induced nuclides such as carbon-14 (half-life: 5730 years) in tree rings or beryllium-10 (half-life: 1.36 million years) in ice cores from polar regions are powerful tools to reconstruct the variations in the cosmic-ray intensity and the solar activity in the past. These nuclides are produced by the nuclear interactions between cosmic rays and the atmosphere of the Earth. Carbon-14 forms carbon dioxide, which is absorbed by trees via photosynthesis, whereas beryllium-10

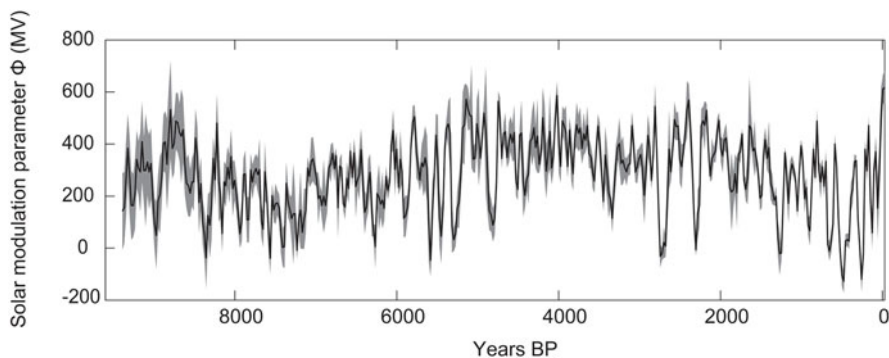


Fig. 13.5 Solar activity during the past 10,000 years reconstructed based on carbon-14 in tree rings and beryllium-10 in multiple ice cores. (Steinhilber et al. 2012)

attaches to aerosols and precipitates on ice sheets in the polar regions or on sediments.

Both nuclides have their strengths and weaknesses as tools for reconstructing past cosmic-ray and solar variations. For example, the signatures of cosmic-ray/solar variations in carbon-14 are significantly attenuated and distorted during its circulation in the carbon cycle, particularly those with a timescale of less than a decade. For precise reconstruction of signatures, the time profile of the production rate needs to be restored using a carbon cycle box model. In contrast, records of carbon-14 obtained from tree rings with definitive visible annual layers enable the reconstruction of the variations in the cosmic-ray intensity and the solar activity with accurate time stamps. This aspect is essential, particularly when the index is used for reconstructing the cycle lengths. Two methods are generally used to determine the absolute ages of tree rings: dendrochronology, which utilizes the temporal variations in tree-ring widths (Douglass 1937, 1946), and searching the carbon-14 concentration peak caused by nuclear bomb tests (Cain and Suess 1976). In recent years, there have also been attempts to utilize the temporal variations in oxygen isotope ratios to determine the ages of tree-ring samples.

In the case of beryllium-10, attenuation in the atmosphere is relatively small; however, its precipitation or deposition processes are occasionally significantly affected by climate variations. Therefore, it is necessary to correct these effects based on climate proxies to obtain an accurate cosmic-ray history. It should be noted that when using ice cores, the obtained records may contain dating uncertainties of several years. It is also possible to obtain beryllium-10 records using annually laminated lake sediments; however, they are highly susceptible to variations in climate and, thus, should be carefully examined.

Therefore, it is important to obtain and compare the records of multiple nuclides for accurate reconstruction of the cosmic-ray intensity and the solar activity. For the past 10,000 years, long-term variations in solar activity have been reconstructed by extracting common signatures from carbon-14 and beryllium-10 records (Fig. 13.5).

For older ages, reconstructions have been achieved mainly using beryllium-10 with a longer half-life (e.g., Horiuchi et al. 2016).

Beryllium-10 allows the reconstruction of cosmic-ray history for the past million years or more. However, when using ice cores, it becomes difficult to achieve annual resolution at high depths owing to the thinning effect of ice layers (Beer 2000). Thus far, annual layers have been traced to approximately 30,000 years ago in the case of Antarctic ice cores (Sigl et al. 2016) and to approximately 60,000 years ago in the case of Greenland ice cores (Svensson et al. 2008).

Recently, it was newly discovered that cosmic-ray intensity can also be reconstructed from the annual layers of carbonate deposits called travertines (Xu et al. 2019; Miyahara et al. 2020). Travertines frequently contain visible annual layers produced by the inflow of soils in rainy seasons. Different from ice sheets, travertines are barely compressed after their formation. Therefore, analyses with high temporal resolution can be achieved even at high depths. Until now, the existence of travertines up to one million years ago has been confirmed (Capezuoli et al. 2014); therefore, beryllium-10 in travertines may enable extending high-resolution records further back in time.

The intensity of galactic cosmic rays (GCRs) arriving at the Earth is generally inversely related to the solar activity level, depending mainly on the intensity of the heliospheric magnetic field and the structure of the Parker spiral (Jokipii and Thomas 1981). As the solar activity increases, the solar wind becomes intensified, and thus, the attenuation level of GCRs increases. In addition, when the spiral structure of the heliospheric magnetic field is significantly developed, the orbit of GCRs, mainly consisting of protons, is altered and the efficiency of energy loss is increased. Owing to these effects, GCRs with energies below a few tens of GeV are modulated in the heliosphere. Based on neutron monitor data, the flux of GCRs varies by 20–25%, associated with solar activity variations. In addition, coronal mass ejections occasionally cause transient decrements in GCRs. This phenomenon is called the Forbush decrease.

In addition to the variations associated with solar activity, GCRs present a 22-year variation related to the reversal of the solar dipole magnetic field (Kota and Jokipii 1983). The large-scale motion of GCRs in the heliosphere is determined by the direction of the heliospheric magnetic field (drift effect), and thus, by the direction of the solar dipole magnetic field (Fig. 13.6). When the polarity of the solar dipole magnetic field is negative, GCRs tend to drift inward along the wavy heliospheric magnetic field. In contrast, GCRs tend to penetrate the polar regions of the heliosphere, when the polarity is positive. These effects cause the waveform of the cosmic-ray variation to be different every other 11-year cycle, resulting in a 22-year cycle. GCRs are more susceptible to the structure of the heliospheric magnetic field when the magnetic polarity of the Sun is negative than when it is positive. It has been suggested that the 22-year component in GCR variations may be particularly pronounced when, for example, the solar activity becomes extremely decreased or increased (Miyahara et al. 2008).

Beryllium-10 records from the Maunder minimum, when sunspots disappeared for several decades, have suggested that the spiral heliospheric magnetic field was

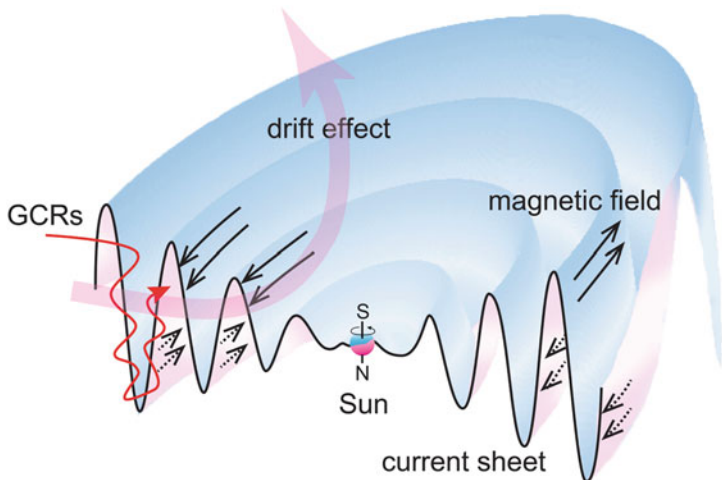


Fig. 13.6 Schematic of the spiral structure of the heliospheric current sheet and orbit of GCRs. Thick arrows indicate directions of meridional circulation of GCRs when the solar dipole magnetic field is negative. Directions of arrows are reversed when the dipole magnetic polarity of the Sun becomes positive

extremely flattened at the solar cycle minima and that the 22-year cycle might have been pronounced at the time (Miyahara et al. 2008; Yamaguchi et al. 2010; Kataoka et al. 2012). An approximately 40% increase in the GCR flux was found at the minima of negative polarity, in addition to decadal-scale variations. Along with the effects of the flattening of the heliospheric magnetic field, there may have been an impact from the outer heliosheath causing the above increase. A better understanding of the structures of the heliosphere and the heliosheath and a highly realistic model of the GCR modulation therein are needed to understand the variability in the GCR flux at the Earth.

Annually resolved records of cosmogenic nuclides provide information on the characteristics of the solar cycles in the past and, thus, are essential for understanding the mechanisms of the long-term solar activity level. It has been suggested that the length of the solar activity cycle may reflect the condition of the meridional circulation in the solar convection zone (Dikpati and Charbonneau 1999). Analysis of the carbon-14 content in tree rings from the Maunder minimum has indicated that the solar cycle might have been lengthened to approximately 14 years (Miyahara et al. 2004). It has also been suggested that this lengthening might have started three cycles before the onset of the Maunder minimum (Miyahara et al. 2021). A similar tendency has been also found for the Spörer minimum (Miyahara et al. 2010; Moriya et al. 2019). Further examinations of the solar cycle lengths for the various types of grand solar minima based on high-precision carbon-14 analyses may elucidate the possible factors determining the magnitude of grand solar minima.

During the past decade, records of cosmogenic nuclides have also been utilized for searching past large-scale solar flare events. Significant increments have been

found in the production rate of carbon-14, e.g., in 774–775 C.E., 993–994 C.E., and 660 B.C.E (Miyake et al. 2012, 2013; O’Hare et al. 2019; Sakurai et al. 2020). Moreover, it has been suggested that they were caused by large-scale solar proton events. For 774–775 C.E. and 993–994 C.E. events, increments in both beryllium-10 and chlorine-36 have been reported based on ice-core analyses (Mekhaldi 2015). It is expected that these records are important not only from astrophysical and space weather perspectives but also as markers to determine the absolute ages of natural materials or the proxy records obtained from them.

13.3 Solar Influence on Climate Observed in Paleoclimate Data

Past climate changes can be examined based on several proxy records. For example, temporal variations in tree-ring widths are frequently used to reconstruct summer-time temperatures. This is because the growth rates of trees are frequently correlated to the temperature in the growing season and are reflected in the widths of annual rings. Occasionally, trees may be more sensitive to the amount of precipitation, depending on the surrounding climatic environment. Therefore, it is essential to determine in advance the meteorological parameters the trees are most susceptible to. Past temperature variations can also be reconstructed by measuring the temperatures in boreholes (Huang et al. 2000). This method is based on the fact that temperature variations at the surface of the Earth are transported to the subsurface by heat conduction. In addition, temperature measurements in the Greenland ice sheet have revealed the temperature history for the past 1000 years (Dahl-Jensen et al. 1998). Although the temperature reconstructions based on drilled holes have a lower temporal resolution, they reflect more directly the thermal history of the surface of the Earth.

Another possible methodology for reconstructing past temperature variation is based on plant physiology. For example, the date of the full bloom of cherry trees is highly correlated with the average temperature in March, and accordingly, temperature fluctuations over the past 1200 years have been reconstructed using diaries preserved in Kyoto (Aono and Kazui 2008). In another case, the number of rainy days was examined based on the weather records in diaries, and the summertime temperature was reconstructed based on their correlation (Mikami 2008). In Europe, records of grape harvest for wine-making were used to reconstruct the temperatures during the past 600 years (García de Cortázar-Atauri et al. 2010). In other cases, variations in the sea surface temperature over hundreds of years have been reconstructed based on Sr/Ca ratios in coral skeletons (Kawakubo et al. 2017).

Long-term temperature variations can be reconstructed, e.g., from analyses of pollen in lake and marine sediments (Nakagawa et al. 2003; Hayashi et al. 2010; Kitaba et al. 2013) and from ice-rafted debris in marine sediments (Bond and Lotti

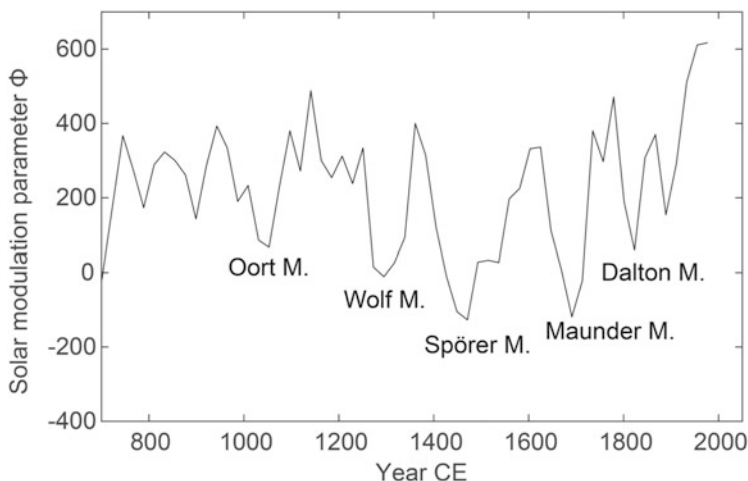


Fig. 13.7 Solar activity minima in the last 1000 years. (Based on Steinhilber et al. 2012)

1995). Oxygen isotope ratios in ice cores have also been commonly used as indicators of climate change (Grootes et al. 1993).

The trends in dry and wet environments can be reconstructed based on the oxygen isotope ratio in stalagmites (Wang et al. 2005). When precipitation increases, the oxygen isotope ratio decreases (amount effect). This tendency allows to reconstruct the amount of precipitation in the past. In recent years, the oxygen isotope ratio of annual tree rings has also been used to reconstruct dry and humid environments. In the case of tree rings, the oxygen isotope ratio in cellulose reflects the amount of precipitation and/or relative humidity (Li et al. 2015).

The relationship between climate and solar activity has long been studied. Various direct and indirect climate records such as temperature, precipitation, and droughts have suggested that periodic variations are synchronized to solar cyclic variations with timescales of a decade to a few millennia. One of the most notable examples is the Little Ice Age, which occurred synchronously with the series of grand solar minima since the late thirteenth century, including the Maunder minimum (Fig. 13.7). Before the Little Ice Age, the climate had been warm for several 100 years, corresponding to a period of Medieval solar activity maximum. It has been suggested that volcanic eruptions such as those of Mount Tambora in 1815 C.E. also contributed to the decrease in temperature during the Little Ice Age (Gao et al. 2008).

The relationship between the weakening of solar activity and cold climate has been further confirmed by research based on ice-rafted debris in deep-sea sediment cores from North Atlantic (Bond et al. 2001). The number of ice-rafted debris reflected a millennial-scale cyclic variation synchronization with 1000/2000-year solar activity cycles throughout the past 10,000 years. An increase in ice-rafted debris in deep-sea sediments implies an increase in the amount of iceberg discharge from the Arctic region and/or the southward expansion of the cold sea surface water.

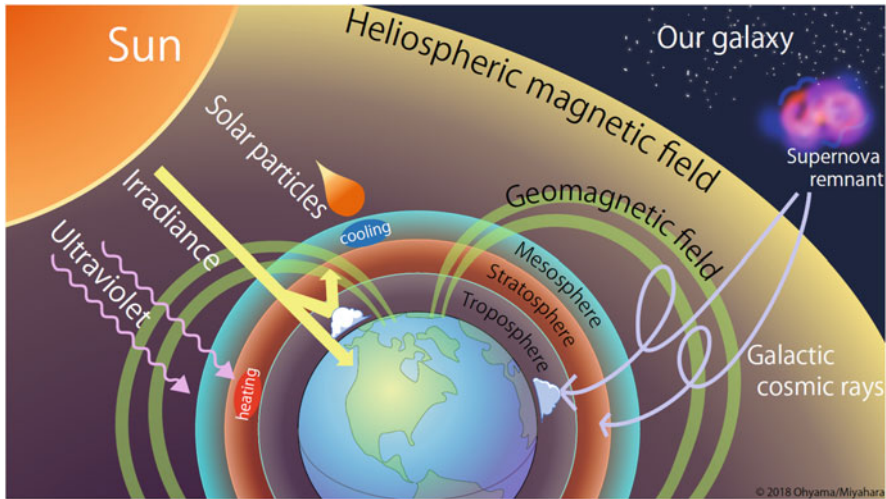


Fig. 13.8 Schematic of pathways of solar influence on the climate system

Similar 1000/2000-year cycles were also found in the last glacial period (Obrochta et al. 2012), suggesting that solar activity had a pronounced influence during the time.

It becomes relatively difficult to identify the solar influence on climate at short timescales; however, studies have suggested the impacts of the 11-year solar cycle (e.g., van Loon et al. 2004; Misios et al. 2019), and even the solar rotation cycle. The rotation of the Sun within a 27-day period causes quasi-cyclic variations in the TSI and UV associated with the migration of sunspots and faculae on the solar surface. The GCR flux also shows similar monthly variations, because coronal mass ejections causing the transient decrements in GCRs originate in sunspots on the solar surface. Impacts of the solar rotation cycle have been found, e.g., in global lightning activity monitored by the Schumann resonance (Sato and Fukunishi 2005), thunderstorm activity in Japan (Muraki et al. 2004; Miyahara et al. 2017) and the United Kingdom (Scott et al. 2014), and in equatorial cloud activity (Takahashi et al. 2010; Hong et al. 2011). The important feature of these impacts is that they are rarely detected during periods of low solar activity. They are only significantly detected when there are many sunspots and monthly variations in solar-related parameters are pronounced. A study on the thunderstorm activity for the past 150 years based on old diaries further confirmed that the impact of the solar rotation cycle becomes stronger as the number of sunspots increases (Miyahara et al. 2018).

The above examples demonstrate that correlations between solar activity and climate or meteorological phenomena have been found on various timescales, although the mechanisms behind the link are poorly understood. There are several possible pathways by which solar activity can influence climate (Fig. 13.8). The simple path is by the TSI variations; however, TSI observations since the late 1970s have revealed that the difference in the TSI between the solar activity maxima and

minima is only approximately 1 W/m^2 . Therefore, it is not highly probable that the TSI variations can explain the observed temperature/precipitation variations, unless a strong positive feedback is identified. Another possible path is by UV radiation, which affects stratospheric temperatures. The other possible candidates are the impacts of solar wind particles on atmospheric chemical reactions and the influence of GCRs on the formation of cloud condensation nuclei and/or on the efficiency of the coalescence of aerosols and cloud particles.

There are a few possible approaches to discriminate the effects of GCRs from other solar-related parameters. For example, examination of the response of climate to the 22-year cycle allows identifying the effects of GCRs (Miyahara et al. 2008; Yamaguchi et al. 2010). It may also be possible to discriminate the impacts of GCRs by focusing on the solar rotation period. Although the amount of solar radiation fluctuates depending on the areas of the sunspots and faculae and their migrations on the solar surface, the variations in GCRs are mainly determined by the crossing of the coronal mass ejections accompanying the strong magnetic field around the Earth. Therefore, the characteristics of monthly-scale variations are slightly different from each other. Comparison of paleo-climate records with the history of the geomagnetic field intensity will also allow understanding the impacts of GCRs on the climate (Kitaba et al. 2013). Searching for the effects of GCR variations at even longer timescales, e.g., the variations with the change in nearby star formation rate, may also provide insight into its role (Shaviv 2002).

It should be noted that there are significant regional differences in the responses of the climate to solar activity. It has been suggested by studies on the Little Ice Age that there existed regions in which the temperature dropped by as much as $2.5 \text{ }^\circ\text{C}$ (Aono and Kazui 2008; Mann et al. 2009), although the globally averaged decrease was only approximately $0.6 \text{ }^\circ\text{C}$. Japan appears to have been one of the most susceptible regions to solar activity variations.

Precipitation also shows significant regional differences in the responses to solar activity. For example, the amount of summertime precipitation increased around the South China Sea during the Little Ice Age, whereas the northern China region has drier condition (Yan et al. 2015). Such a regional pattern may reflect the changes in atmospheric circulation around the time. Oxygen isotope ratios in Japanese tree rings indicated that precipitation increased during the Little Ice Age in central Japan, particularly at the end of the event (Sakashita et al. 2017). A delay in the responses of the precipitation to solar activity implies that the mechanism of Sun–climate connection involves changes in the sea surface temperature. Examination of the spatial pattern in the responses of the climate to the solar activity would provide insight on the process of the solar influence on the climate system.

Acknowledgements The Precision Solar Photometric Telescope (PSPT) was maintained and operated at Mauna Loa Solar Observatory from 1998 to 2015 by the High Altitude Observatory/National Center for Atmospheric Research (HAO/NCAR). The data was processed at and is served to the community by the Laboratory for Atmospheric and Space Physics (LASP) at the University of Colorado, Boulder. The PSPT effort was supported by the National Science Foundation (NSF).

References

- Aono, Y., Kazui, K.: Phenological data series of cherry tree flowering in Kyoto, Japan, and its application to reconstruction of springtime temperatures since the 9th century. *Int. J. Climatol.* **28**, 905–914 (2008)
- Beer, J.: Long-term indirect indices of solar variability. *Space Sci. Rev.* **94**, 53–66 (2000)
- Bertello, L., Ulrich, R.K., Boyden, J.E.: The Mount Wilson Ca ii K Plage index time series. *Sol. Phys.* **264**, 31–44 (2010)
- Bond, G.C., Lotti, R.: Iceberg discharges into the North Atlantic on millennial time scales during the last glaciation. *Science.* **267**, 1005–1010 (1995)
- Bond, G., et al.: Persistent solar influence on North Atlantic climate during the Holocene. *Science.* **294**, 2130–2136 (2001)
- Cain, W.F., Suess, H.E.: Carbon 14 in tree rings. *J. Geophys. Res.* **81**, 3688–3694 (1976)
- Capeczuoli, E., Gandin, A., Pedley, M.: Decoding tufa and travertine (fresh water carbonates) in the sedimentary record: the state of the art. *Sedimentology.* **61**, 1–21 (2014)
- Chatterjee, S., et al.: A butterfly diagram and Carrington maps for century-long CA II K spectroheliograms from the Kodaikanal observatory. *Astrophys. J.* **827**, id87 (2016)
- Chatzistergos, H., et al.: Analysis of full disc ca II K spectroheliograms. II. Towards an accurate assessment of long-term variations in plage areas. *Astron. Astrophys.* **625**, 69 (2019)
- Dahl-Jensen, D., et al.: Past temperatures directly from the Greenland ice sheet. *Science.* **282**, 268–271 (1998)
- Dikpati, M., Charbonneau, P.: A Babcock-Leighton flux transport dynamo with solar-like differential rotation. *Astrophys. J.* **518**, 508–520 (1999)
- Douglass, A.E.: Tree rings and chronology. *Univ. Arizona Bull.* **8** (1937)
- Douglass, A.E.: Precision of ring dating in tree-ring chronologies. *Univ. Arizona Bull.* **17** (1946)
- Elias, I., et al.: Trends in the solar quiet geomagnetic field variation linked to the Earth’s magnetic field secular variation and increasing concentrations of greenhouse gases. *J. Geophys. Res.* **115**, A08316 (2010)
- Ermolli, I., et al.: The digitized archive of the Arcetri spectroheliograms. Preliminary results from the analysis of ca II K images. *Astron. Astrophys.* **499**, 627–632 (2009)
- Ermolli, I., et al.: Recent variability of the solar spectral irradiance and its impact on climate modelling. *Aomos. Chem. Phys.* **13**, 3945–3977 (2013)
- Foukal, P., et al.: A century of solar ca ii measurements and their implication for solar UV driving of climate. *Sol. Phys.* **255**, 229–238 (2009)
- Fröhlich, C.: Evidence of a long-term trend in total solar irradiance. *Astron. Astrophys.* **501**, L27–L30 (2009)
- Gao, C., Robock, A., Ammann, C.: Volcanic forcing of climate over the past 1500 years: an improved ice core-based index for climate models. *J. Geophys. Res.* **113**, D23111 (2008)
- García de Cortázar-Atauri, I., et al.: Climate reconstructions from grape harvest dates: methodology and uncertainties. *Holocene.* **20**, 599–608 (2010)
- Grootes, P.M., et al.: Comparison of oxygen isotope records from the GISP2 and GRIP Greenland ice cores. *Nature.* **366**, 552–554 (1993)
- Hanaoka, Y.: Long-term synoptic observations of the sun at the National Astronomical Observatory of Japan. *J. Phys. Conf. Ser.* **440**, 012041 (2013)
- Hansen, J., et al.: Assessing “dangerous climate change”: required reduction of carbon emissions to protect young people, future generations and nature. *PLoS One.* **8**, e81648 (2013)
- Hasan, S.S., et al.: Solar physics at the Kodaikanal observatory: a historical perspective. A historical perspective. *Astrophys. Space Sci. Proc.* **19**, 12 (2010)
- Hayashi, R., Takahara, H., Hayashida, A., Takemura, K.: Millennial-scale vegetation changes during the last 40,000 yr based on a pollen record from Lake Biwa, Japan. *Quater. Res.* **74**, 91099 (2010)
- Hong, P.K., et al.: Implications for the low latitude cloud formations from solar activity and the quasi-biennial oscillation. *J. Atmos. Sol. Terr. Phys.* **73**, 587–591 (2011)

- Horiuchi, K., et al.: Multiple ^{10}Be records revealing the history of cosmic-ray variations across the Iceland Basin excursion. *Earth Planet. Sci. Lett.* **440**, 105–114 (2016)
- Huang, S., Pollack, H.N., Shen, P.-Y.: Temperature trends over the past five centuries reconstructed from borehole temperatures. *Nature*. **403**, 756–758 (2000)
- Jokipii, J.R., Thomas, B.: Effects of drift on the transport of cosmic rays IV - modulation by a wavy interplanetary current sheet. *Astrophys. J.* **243**, 1115–1122 (1981)
- Kakuwa, J., Ueno, S.: Investigation of the long-term variation of solar CaII K intensity. I. Density-to-intensity calibration formula for historical photographic plates. *Astrophys. J. Suppl. Ser.* **254**, id44 (2021)
- Kakuwa, J., Ueno, S.: Investigation of the long-term variation of solar CaII K intensity. II. Reconstruction of solar UV irradiance. *Astrophys. J.* **928**, id97 (2022)
- Kataoka, R., Miyahara, H., Steinhilber, F.: Anomalous ^{10}Be spikes during the maunder minimum: possible evidence for extreme space weather in the heliosphere. *Space Weather*. **10**, S11001 (2012)
- Kawakubo, Y., Alibert, C., Yokoyama, Y.: A reconstruction of subtropical western North Pacific SST variability back to 1578, based on a *Porites* coral Sr/Ca record from the northern Ryukyus, Japan. *Paleoceanography*. **32**, 1352–1370 (2017)
- Kitaba, I., et al.: Midlatitude cooling caused by geomagnetic field minimum during polarity reversal. *Proc. Natl. Acad. Sci.* **110**, 1215–1220 (2013)
- Kitai, R. et al.: Digital Archiving of Solar Synoptic Observation (1) Project Outline and Meta-Data Archiving. Technical Reports from Kwasan and Hida Observatories, Graduate School of Science, Kyoto University 2–2 (2014)
- Kota, J., Jokipii, J.R.: Effects of drift on the transport of cosmic rays. VI - a three-dimensional model including diffusion. *Astrophys. J.* **265**, 573–581 (1983)
- Krivova, N.A., Vieira, L.E.A., Solanki, S.K.: Reconstruction of solar spectral irradiance since the maunder minimum. *J. Geophys. Res.* **115**, A12112 (2010)
- Lean, J.: Solar ultraviolet irradiance variations - a review. *J. Geophys. Res.* **92**, 839–868 (1987)
- Lean, J.: The sun's variable radiation and its relevance for earth. *Annu. Rev. Astrophys.* **35**, 33–67 (1997)
- Li, Z., Nakatsuka, T., Sano, M.: Tree-ring cellulose $\delta^{18}\text{O}$ variability in pine and oak and its potential to reconstruct precipitation and relative humidity in Central Japan. *Geochem. J.* **49**, 125–137 (2015)
- Mann, M.E., et al.: Global signatures and dynamical origins of the little ice age and medieval climate anomaly. *Science*. **326**, 1256–1260 (2009)
- Mekhaldi, F.: Multiradionuclide evidence for the solar origin of the cosmic-ray events of AD 774/5 and 993/4. *Nature Commun.* **6**, 8611 (2015)
- Mikami, T.: Climatic variations in Japan reconstructed from historical documents. *R. Met. Soc.* **63**, 190–193 (2008)
- Misios, S., et al.: Slowdown of the Walker circulation at solar cycle maximum. *Proc. Natl. Acad. Sci.* **116**, 7186–7191 (2019)
- Miyahara, H., et al.: Cyclicity of solar activity during the maunder minimum deduced from radiocarbon content. *Sol. Phys.* **224**, 317–322 (2004)
- Miyahara, H., Yokoyama, Y., Masuda, K.: Possible link between multi-decadal climate cycles and periodic reversals of solar magnetic field polarity. *Earth Planet. Sci. Lett.* **272**, 290–295 (2008)
- Miyahara, H., et al.: Is the sun heading for another maunder minimum? -precursors of the grand solar minima. *J. Cosmol.* **8**, 1970–1982 (2010)
- Miyahara, H., et al.: Solar 27-day rotational period detected in a wide-area lightning activity in Japan. *ANGEО Commun.* **35**, 583–588 (2017)
- Miyahara, H., et al.: Solar rotational cycle in lightning activity in Japan during the 18–19th centuries. *ANGEО Commun.* **36**, 633–640 (2018)
- Miyahara, H., et al.: Measurement of beryllium-10 in terrestrial carbonate deposits from South China: a pilot study. *Nucl. Instrum. Methods Phys. Res. B.* **464**, 36–40 (2020)

- Miyahara, H., et al.: Gradual onset of the maunder minimum revealed by high-precision carbon-14 analyses. *Sci. Rep.* **11**, 5482 (2021)
- Miyake, F., et al.: A signature of cosmic-ray increase in AD 774–775 from tree rings in Japan. *Nature*. **486**, 240–242 (2012)
- Miyake, F., Masuda, K., Nakamura, T.: Another rapid event in the carbon-14 content of tree rings. *Nature Comm.* **4**, 1748 (2013)
- Moriya, T., et al.: A study of variation of the 11-year solar cycle before the onset of the Sporer minimum based on annually measured 14C content in tree rings. *Radiocarbon*. **61**, 1749–1754 (2019)
- Muraki, Y., et al.: Effects of atmospheric electric fields on cosmic rays. *Phys. Rev. D*. **69**, 123010 (2004)
- Nakagawa, T., Kitagawa, H., Yasuda, Y., Tarasov, P.E., Nishida, K., Gotanda, K., Sawai, Y.: Asynchronous climate changes in the North Atlantic and Japan during the last termination. *Science*. **299**, 688–691 (2003)
- O’Hare, P., et al.: Multiradionuclide evidence for an extreme solar proton event around 2,610 B.P. (~660 BC). *Proc. Natl. Acad. Sci.* **116**, 5961–5966 (2019)
- Obrochta, S.P., Miyahara, H., Yokoyama, Y., Crowley, T.J.: A re-examination of evidence for the North Atlantic “1500-year cycle” at site 609. *Quat. Sci. Rev.* **55**, 23–33 (2012)
- Sakashita, W., et al.: Hydroclimate reconstruction in Central Japan over the past four centuries from tree-ring cellulose $\delta^{18}O$. *Quat. Int.* **455**, 1–7 (2017)
- Sakurai, H., et al.: Prolonged production of 14C during the ~660 BCE solar proton event from Japanese tree rings. *Sci. Rep.* **10**, 660 (2020)
- Sato, M., Fukunishi, H.: New evidence for a link between lightning activity and tropical upper cloud coverage. *Geophys. Res. Lett.* **32**, L12807 (2005)
- Schrijver, C.J., et al.: The minimal solar activity in 2008–2009 and its implications for long-term climate modeling. *Geophys. Res. Lett.* **38**, L06701 (2011)
- Scott, C.J., et al.: Evidence for solar wind modulation of lightning. *Environ. Res. Lett.* **9**, 055004 (2014)
- Shaviv, N.J.: Cosmic ray diffusion from the galactic spiral arms, iron meteorites, and a possible climatic connection. *Phys. Rev. Lett.* **89**, 089901 (2002)
- Shimojo, M., et al.: Variation of the solar microwave spectrum in the last half century. *Astrophys. J.* **848**, id62 (2017)
- Shinori, A., et al.: Long-term variation in the upper atmosphere as seen in the geomagnetic solar quiet daily variation. *Earth Planets Space*. **66**, id155 (2014)
- Sigl, M., et al.: The WAIS divide deep ice core WD2014 chronology – part 2: annual-layer counting (0–31 ka BP). *Clim. Past*. **12**, 769–786 (2016)
- Solanki, S., et al.: Solar irradiance variability and climate. *Annu. Rev. Astrophys.* **51**, 311–351 (2013)
- Steinhilber, F., Beer, J., Fröhlich, C.: Total solar irradiance during the Holocene. *Geophys. Res. Lett.* **36**, L19704 (2009)
- Steinhilber, F., et al.: 9,400 years of cosmic radiation and solar activity from ice cores and tree rings. *Proc. Natl. Acad. Sci.* **109**, 5967–1971 (2012)
- Svensson, K., et al.: A 60 000 year Greenland stratigraphic ice core chronology. *Clim. Past*. **4**, 47–57 (2008)
- Takahashi, Y., et al.: 27-day variation in cloud amount and relationship to the solar cycle. *Atmos. Chem. Phys.* **10**, 1577–1584 (2010)
- Tapping, K.F., Charrois, D.: P.: limits to the accuracy of the 10.7-centimeter flux. *Sol. Phys.* **150**, 305–315 (1994)
- van Loon, H., Meehl, G.A., Arblaster, J.M.: A decadal solar effect in the tropics in July–August–J. *Atmos. Sol.-Terr. Phys.* **66**, 1767–1778 (2004)

- Wang, Y., et al.: The Holocene Asian monsoon: links to solar changes and North Atlantic climate. *Science*. **308**, 854–857 (2005)
- Xu, H., et al.: High-resolution records of ^{10}Be in endogenic travertine from Baishuitai, China: a new proxy record of annual solar activity? *Quat. Sci. Rev.* **216**, 34–46 (2019)
- Yamaguchi, T., Yokoyama, Y., Miyahara, H., Sho, K., Nakatsuka, T.: Synchronized northern hemisphere climate change and solar magnetic cycles during the maunder minimum. *Proc. Natl. Acad. Sci.* **107**, 20697–20702 (2010)
- Yan, H., et al.: Dynamics of the intertropical convergence zone over the western Pacific during the little ice age. *Nat. Geo.* **8**, 315–320 (2015)